41st AIAA/ASME/SAE/ASEE Joint Propulsion Conference & Exhibit AIAA-2005-4143
Tucson, Arizona
10-13 July 2005

Flow Field Measurements in a Counter-Swirling Spray Combustor

J. Colby*, S. Menon†, J. Jagoda‡
School of Aerospace Engineering
Georgia Institute of Technology, Atlanta, GA, 30332-0150

To adhere to the current requirements for NO_x emissions in combustion systems, modern land and air based gas turbine engines often operate in the lean regime. While operating near the lean blowout limit does reduce harmful emissions, combustor stability is sacrificed and extinction becomes a major concern. To understand the characteristics of lean operation, an experimental study was conducted to map the time averaged flow field in a typical industrial, counter-swirling, liquid fuel combustor. 2-D mean velocities and Reynolds stresses were measured throughout the combustor. Measurements taken for both the non-reacting and reacting flow fields enable a direct analysis of the result of heat addition on a turbulent swirling flow field. To further understand the overall flow field, liquid droplet diameter measurements were taken to determine the spray characteristics. For the reacting flow, chemical composition at the combustor exit was also measured. From these, an understanding of the reacting flow field will aid in predicting lean blowout events.

Nomenclature

D_{32}	=	Sauter mean diameter
D_o	=	rated fuel nozzle Sauter mean diameter
k	=	2-D turbulent kinetic energy
l_m	=	mixing length
P_{AIR}	=	air pressure upstream of counter-swirler
R_o	=	effective fuel nozzle radius
Re_0	=	inflow Reynolds number
S	=	swirl number
T_{AIR}	=	air temperature upstream of counter-swirler
U	=	axial mean velocity
U_o	=	bulk velocity
u	=	axial root-mean-square velocity
u'	=	axial fluctuating velocity
u^*	=	velocity scale based on turbulent kinetic energy
$u'v'$	=	2-D Reynolds shear stress
V	=	vertical mean velocity
v	=	vertical root-mean-square velocity
v'	=	vertical fluctuating velocity
ε	=	dissipation of turbulent kinetic energy
Φ	=	overall equivalence ratio
υ_T	=	turbulent viscosity

I. Introduction

IN the fuel lean limit, combustor stability is reduced as inflow velocity fluctuations cause localized extinction events. Based on several parameters, including spray characteristics and both mixing and residence times, these

* Graduate Research Assistant, AIAA Student Member.
† Professor, AIAA Associate Fellow.
‡ Professor, AIAA Associate Fellow.

localized events can lead to the global extinction of the flame. These global extinction events, or lean blowouts, are both costly and dangerous. In land based turbines, an extinction event leads to a stoppage in power output; a major problem for an electricity or energy company. For aircraft turbine engines, an extinction event at altitude also means a loss of power, necessary for thrust generation. Further, extinction events imply the production of large quantities of unburned hydrocarbons, both inefficient and harmful.

To better understand the characteristics of lean operation, an experimental study was conducted to map the time averaged flow field in a typical industrial type, counter-swirl stabilized, liquid fuel combustor. Using a TSI Phase Doppler Particle Analyzer (PDPA)/Laser Doppler Velocimeter (LDV) system, 2-D mean and fluctuating velocities, as well as Reynolds stresses, were measured throughout the combustor. These measurements were taken along the horizontal and vertical centerlines, shown in Fig. 1 (Section A-A), for both non-reacting and reacting flow fields, enabling a direct analysis of the result of heat addition on a turbulent swirling flow field. For all gas phase measurements, aluminum oxide was used for the seed particles. To improve understanding of the overall flow field, liquid droplet diameter measurements were taken to determine the spray characteristics. In addition to the droplet diameter statistics, the aerodynamic properties of the droplets were measured. From this, the relative motion between the droplets and the gas phase flow was determined. To complete this study, the gas composition at the combustor exit was measured, with a focus on CO and NO_x concentrations.

In all of the experimental results presented, liquid Jet-A was atomized using a pressure simplex nozzle. The overall equivalence ratio for these tests, $\Phi \sim 0.4$, is very close to the lean blowout limit, measured experimentally as $\Phi \sim 0.35$ for this geometry. A fixed pressure drop across the swirler of 4.25 % of the upstream pressure is maintained, in good agreement with the typical values used in modern combustor design[1]. The swirler geometry includes a primary, axial, curved vane swirler for the fuel spray, and a secondary, radial swirler for the main air flow, shown schematically in Fig. 1. Dilution holes throughout the dump plate also allow small amounts of non-swirled air into the combustion chamber.

From the current measurements, a more complete understanding of the complex reacting flow field is obtained. In addition, the impact of heat release on the ambient gas phase can be clearly identified, with particular emphasis on the initial droplet distributions and trajectories. Exhaust gas measurements provide insight into combustion performance, while the characteristics of lean operation are highlighted with measurements near the lean blowout limit.

Given the large costs associated with full scale test combustors, the design of valid numerical models is essential for the future of combustor design. Further, the accurate prediction and control of these lean blowout events is essential for dynamic control of lean operation[2]. With these measurements, progress will be made in accurately predicting lean blowout events numerically while providing a deeper understanding of the flow dynamics associated with extinction. Used together, future combustors can be designed with low emission characteristics and large

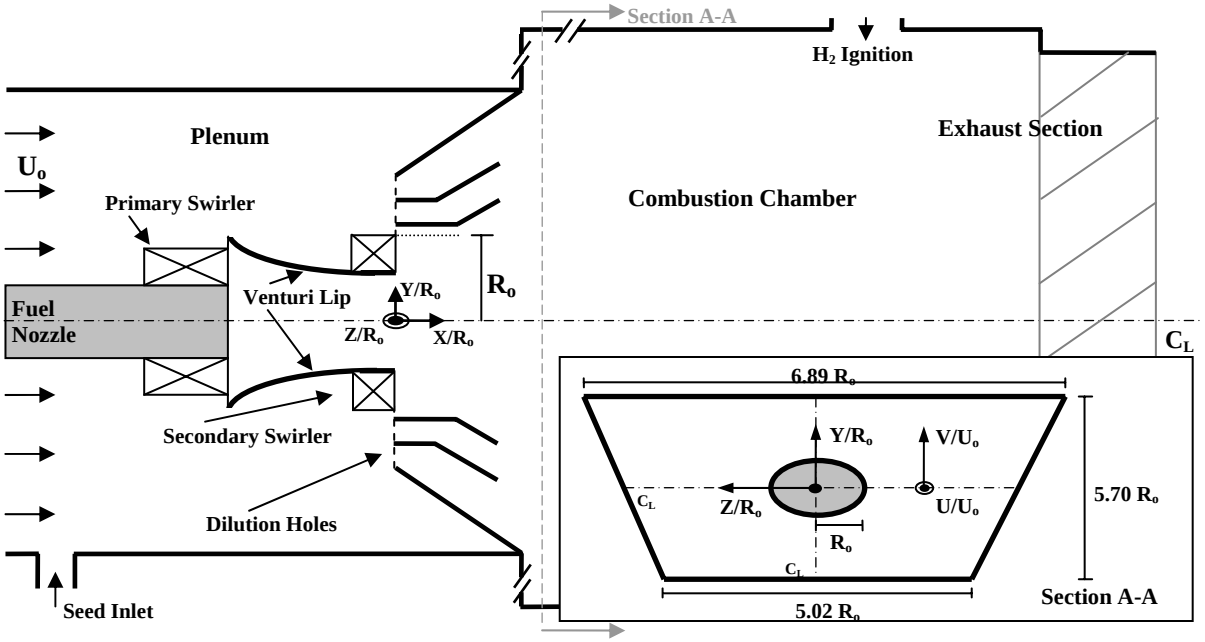

Figure 1. Schematic of the experimental set-up, the counter-swirl burner, and the combustion chamber.

stability limits, ideal for both land and air based turbine engines.

In this paper, we present experimental results from an industrial type, counter-swirl burner operating at idle conditions. The goal of this research is to establish a database for Large Eddy Simulation (LES) validation in such complex flows[3]. A discussion of the experimental equipment, as well as operating conditions, is given in Section II. Results and discussion are given in Section III, followed by a brief conclusion.

II. Experimental Facility

All research aforementioned was conducted at the Georgia Institute of Technology Aerospace Combustion Laboratory on a counter-swirl combustor designed to model a commercial airline engine, shown schematically above in Fig 1. Both the hardware and instrumentation are described below.

A. Hardware

Regulated air, supplied at 125 psig (0.86 MPa), passes through an electrical heater to enable preheating. This preheated air enters a settling chamber, or plenum, for flow straightening, and then dumps in to the combustion chamber through the double annular swirler. A seed inlet well upstream of the swirler allows for adequate mixing of the aluminum oxide particles, mean solid diameter ~ 5 μm, necessary for LDV measurements. As shown schematically in Fig. 1 (Section A-A), the combustion chamber is symmetric about the vertical centerline, with a trapezoidal cross-section. Liquid fuel, Jet-A[4], is delivered using a pressure atomizing fuel nozzle with rated SMD ~ 40 μm at 100 psig (0.69 MPa). A water cooled hydrogen injection system provides ignition and a calibrated turbine flowmeter allows precise measurement of the fuel mass flow rate. The chamber walls are made of fused silica to allow full optical access of the combustion downstream of the swirler lip. Further, top and bottom windows allow full access to the core combustion region. The combustor is mounted on a 3-D traverse, allowing measurement throughout the experimental domain.

B. Instrumentation

For all work presented, the following properties were measured: temperatures, pressures, exhaust gas concentrations, aerodynamic variables, and droplet statistics. The specific capabilities of the experimental set-up are addressed below, including a short note on droplet sizing.

Inlet, steady state, and exhaust gas temperature measurements were made with Omega K-type thermocouples. The total mass flow rate of air was determined by the pressure drop across the swirler, 4.25% of the upstream pressure, and derived from a calibrated rotameter/pressure gage system upstream. The mass flow rate of liquid Jet-A was measured using a viscosity calibrated, digital, turbine flowmeter. Steady state operating conditions are shown in Table 1, with known uncertainties given. The mean Reynolds number, based on the bulk velocity and effective fuel nozzle diameter, is $Re_0 \sim 5x10^4$. For these flow conditions, the overall equivalence ratio, $\Phi = 0.4 \pm 0.01$, with a thermal load of 35 kW.

P_{AIR}	0.25 MPag	± 0.007 MPag
T_{AIR}	380 K	± 1 K
$\dot{m}_{AIR}$	30.5 g/s	0.1 g/s
P_{FUEL}	0.17 Mpag	± 0.007 MPag
$\dot{m}_{FUEL}$	0.750 g/s	± 0.005 g/s

Table 1. Steady State Operating Conditions

All flow velocity and droplet measurements were made with a 2-D TSI PDPA/LDV system. An argon-ion laser was used, with the 514.5 nm and 488 nm lines chosen for the axial and vertical measurements, respectively. The transmitting optics have a focal length, f = 363 mm, and beam separation, b = 40 mm for both channels. The fringe spacing is thus 4.68 μm and 4.44 μm, respectively. A standard Bragg cell provides frequency modulation at 40 MHz to a single beam on each channel, while real time histograms are monitored using the Flowsizer software provided[5]. A band pass filter and downmixing allow the final signal conditioning. The detailed analysis of droplet behavior in the near injector region was performed using the PDPA system at an off-axis receiving angle of 30°. A number of relevant droplet diameters are calculated numerically by the TSI Flowsizer software, including the mass and volume mean diameters. This study, however, will focus on the Sauter Mean Diameter (SMD), given as the diameter of a droplet with the same volume to surface area ratio as that of the entire spray:

$$SMD \ : \quad D_{32} = \Sigma\left(D^3\right)/\Sigma\left(D^2\right) \tag{1}$$

Since the SMD is representative of the entire spray at a given location, it can be considered a global mean property, which should correlate with other spray combustors. Further, its wide usage across the fields of spray

combustion and droplet theory enables the direct comparison of the experimental results shown here with other work in these fields.

Gas composition measurements were made with a HORIBA PG-250 Gas Analyzer downstream of the exhaust section, $X/R_o \sim 22$. Measurements focused on the NO_x ($NO + NO_2$) and CO concentrations across the horizontal centerline. NO_x measurements were made using the chemiluminescence method and a photodiode, while CO concentrations were determined from an infrared analyzer[6]. Both of these measurements were then corrected to 15% O_2 to enable comparison.

III. Results/Discussion

Time-averaged experimental measurements were obtained using the system described above, with a focus on the horizontal (Z/R_o) and vertical (Y/R_o) centerlines at various downstream (X/R_o) locations, seen in Fig. 1. In the following, both reacting and non-reacting results are shown together, with a discussion of the non-reacting case first. For all results presented, these normalization constants were used: $R_o = 13.7$ mm, $U_o = 45.9$ m/s, $D_o = 40$ μm.

A. Non-Reacting Gas Phase

To understand the effects of droplet spray and heat addition in a counter-swirl stabilized spray combustor, the conditions of the non-reacting flow field must be well characterized. At operational flow conditions, the centerline axial mean velocity downstream is given in Fig. 2. The downstream evolution of the axial and vertical mean velocities, without spray or combustion, is shown in Figs. 3 and 4, while the axial and vertical rms velocity evolutions are shown in Figs. 5 and 6. These non-reacting gas phase measurements are plotted as open squares.

The non-reacting gas phase shows many of the expected properties of a flow field with large swirl number, S, the ratio of the tangential flux of angular momentum to the axial thrust. For values of S greater than the critical swirl number, a recirculating flow is established[7]. The presence of a large recirculation region, or vortex breakdown bubble, is seen clearly in both Figs. 2 and 3, and $S > 0.6$ is assumed[7]. In the near-injector region, $X/R_o = 1.60$, where swirl effects are the most pronounced, the flow is highly negative in the core region of the flow, while the external flow is highly positive. The static pressure drop across the swirl burner accelerates the flow, while the adverse pressure gradient associated with the large fraction of angular momentum imparted through the swirler drives the recirculating flow. As the flow expands downstream of the swirler it is clear that the width of the breakdown bubble increases. At three and four nozzle radii downstream the bubble appears to extend across the entire horizontal flow field. While this result appears inconsistent with mass conservation, the three dimensional nature of the flow field and combustor geometry may allow for it. As the third velocity component is not measured, and the cross-sectional geometry is of non-constant area ratio, the flow expanding into the combustion volume traveling in the Y/R_o direction (shown in Fig. 3), should account for the remaining mass flow. Further, previous results suggest that large recirculation regions, "…occupying up to 80% of the exit area of the nozzle and recirculating more than the input mass-flow rates…" are common in high swirl flows[8]. By eleven nozzle radii, the vortex breakdown bubble is closed. The length of this breakdown bubble is clarified in Fig. 2. The axial mean velocity is zero near $X/R_o \sim 11$, evidence of the stagnation point associated with the end of the vortex bubble. Beyond this region, the flow is entirely positive and nearly uniform. Outside of the combustion chamber, $X/R_o \sim 22$, the flow shows this uniformity, with the entrainment of quiescent air distorting the flow field for $Z/R_o > 2$, seen in Fig. 3. It should be noted that the flow experiences a small, abrupt, acceleration through the exhaust region, responsible for the slight asymmetries seen in the exhaust gas profiles.

The swirling nature of the flow is further verified in Fig. 4, where the clock-wise rotation, from a downstream view of the swirler face, is clear. The large vertical velocities continue to $X/R_o \sim 4$, even increasing slightly in the outer regions. At larger downstream distances, the swirl component decreases, with the exception of a slight increase due to the exhaust contraction, as mentioned above. While these results agree well with prior swirling flow research[7,9,10,11], they do not clearly show the counter-swirling nature of the design geometry. The primary swirler, coincident with the fuel nozzle, has little effect on the non-reacting gas phase. In the near nozzle region, $X/R_o = 1.31$, some counter-rotation can be seen near $Z/R_o \sim -2$. However, the effect is small as the velocity does not change direction. Instead, the secondary, clockwise swirl damps the primary swirl. It is assumed that the primary, counter-rotating features would be visible further upstream, at locations $X/R_o < 1.31$; however, optical access is restricted.

Figures 5 and 6 show the axial and vertical rms velocities, respectively, which agree well with previous research[9,12]. The large values near the injector, over 50% of the mean value, confirm the high turbulence intensity downstream of the swirler geometry. These regions of maximum rms velocity correspond to the shear layer present at the vortex bubble edge. The rapid decay of this turbulence downstream is shown clearly in the dramatic reduction of the rms velocity, even at distances as short at 3 nozzle radii. It is also important to note the small rms fluctuations

throughout the combustor's central region. This can be attributed directly to the stability of the core of the break down bubble.

With combustion, it is clear that the dynamics of this non-reacting recirculating region will play a key role in both combustion performance and efficiency. It is also clear that the nozzle characteristics, mainly the spray angle and D_{32}, will contribute significantly to the combustion dynamics, particularly the local heat release rates.

B. Reacting Gas Phase

Velocity measurements of the reacting flow field are also presented in Figs. 3 to 6, while the axial mean velocity downstream along the combustor centerline is seen in Fig. 2. These reacting gas phase measurements are shown as closed circles. From these figures, the effects of heat release on the counter-rotating flow field are clear. Results presented here agree well with previous studies of counter-swirl combustion, while the influence of such lean combustion, $\Phi \sim 0.4$, is not seen in the mean and rms velocity profiles.

Profiles of the axial mean velocity downstream, seen in Figs. 2 and 3, clearly show the presence of a large vortex breakdown bubble due to the swirling nature of the flow. However, the size, shape, and magnitude of this recirculating region change substantially with the addition of heat associated with combustion. In the near-injector region, $X/R_o = 1.60$, seen in Fig. 3, the flow shows the central negative velocity region surrounded by large positive values, similar to the non-reacting phase. However, there is a large reduction in the recirculating region size. In the reacting case, the negative velocities are confined to a region less than one nozzle radius across. In the non-reacting case, however, this region spans almost 3 nozzle radii. The reacting flow also shows a larger positive flow region, with mean axial velocities nearly twice those seen in the non-reacting flow. These two large scale changes to the flow field can be attributed directly to the volumetric expansion of the local gas phase due to the large heat release rates. The axial component of the velocity is strongly influenced by this expansion, pinching the vortex bubble closed near the fuel nozzle, while significantly increasing the net flux of axial momentum. Both the bubble pinching and momentum increase are seen clearly downstream, as the recirculation region is never more than two nozzle radii wide and has completely closed well before $X/R_o = 10.21$, seen in Fig 2. Both of these reacting results differ from the non-reacting case, where the bubble is more than 2½ radii wide, with negative velocities persisting beyond $X/R_o \sim 10$. Reacting exhaust gas velocities are more than twice that of the non-reacting gas, additional evidence of the kinetic energy addition associated with the heat release upstream.

The influence of the combustion process in the near-injector region is shown in Fig. 4 by the change in the mean vertical velocity component at $X/R_o = 1.31$ and $X/R_o = 1.60$. The primary, central, counter-swirl of the combustor becomes apparent with addition of the liquid phase droplets and combustion. While not symmetric, the core region of anti-clockwise rotation can be seen, centered to the right side of the combustor fuel nozzle when viewed from downstream. This counter-rotation quickly decays downstream, no longer evident at $X/R_o = 2.92$. The measurement of this inner rotation suggests that the primary swirl plays an important role in the combustion process through spray-shear interactions. The addition of heat to the flow, with the subsequent axial flow expansion, further enabled the measurement of the counter-swirl nature of this flow.

Downstream, the increase in fluctuating velocity associated with the two-phase flow and the turbulent diffusion flame, discussed below, forces the rapid decay of this counter-rotating flow field to one similar to that seen in the non-reacting gas farther downstream. Note, however, that the exhaust gas at $X/R_o = 22.16$ shows higher swirl in the reacting case, a direct result of the increased flow effects due to the abrupt area change. In addition, the larger kinetic energy associated with the post combustion products leads to a significant increase in both exhaust gas velocity components.

Axial and vertical rms velocities are presented for the reacting gas phase in Figs. 5 and 6. Similar to the mean velocities, the rms results are substantially different with combustion. Most importantly, the core region of the flow field no longer shows the small rms velocities seen previously. Instead, the fluctuating velocity is spread across the horizontal combustor centerline, with a reduction in the peak values near the injector, shown in Fig. 5. This shift in the rms distribution implies active mixing of the liquid and gas phase downstream of the venturi lip (see Fig. 1), which contributes significantly to the increase in velocity fluctuations along the combustor centerline downstream. Closer inspection also reveals an increase in the total rms velocity, evidencing the increase in turbulence associated with the combustion process. At every location downstream, the reacting gas phase shows larger axial rms velocities, further evidence of increased turbulent mixing. While the vertical rms velocities in Fig. 6 show a similar trend at $X/R_o = 1.60$, the rms fluctuations are rapidly damped beyond this location. Given the large amount of tangential momentum imparted to the droplets, this rapid damping of vertical rms velocity may be due to droplet-gas phase interactions smoothing out local fluctuations in the shear layer downstream. Both the re-distribution of fluctuating axial velocity and the damping of vertical, or angular, fluctuating velocity across the combustion cross-section were shown in a similar experimental study[12].

For **Figures 2** through **7**:

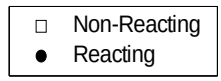

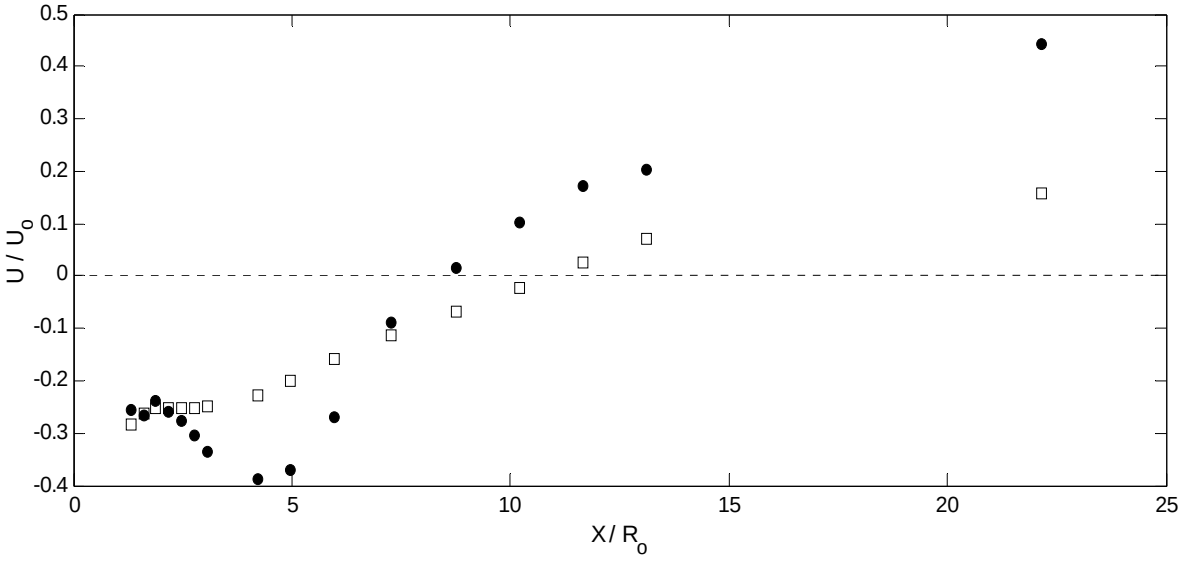

Figure 2. Axial mean velocity centerline downstream.

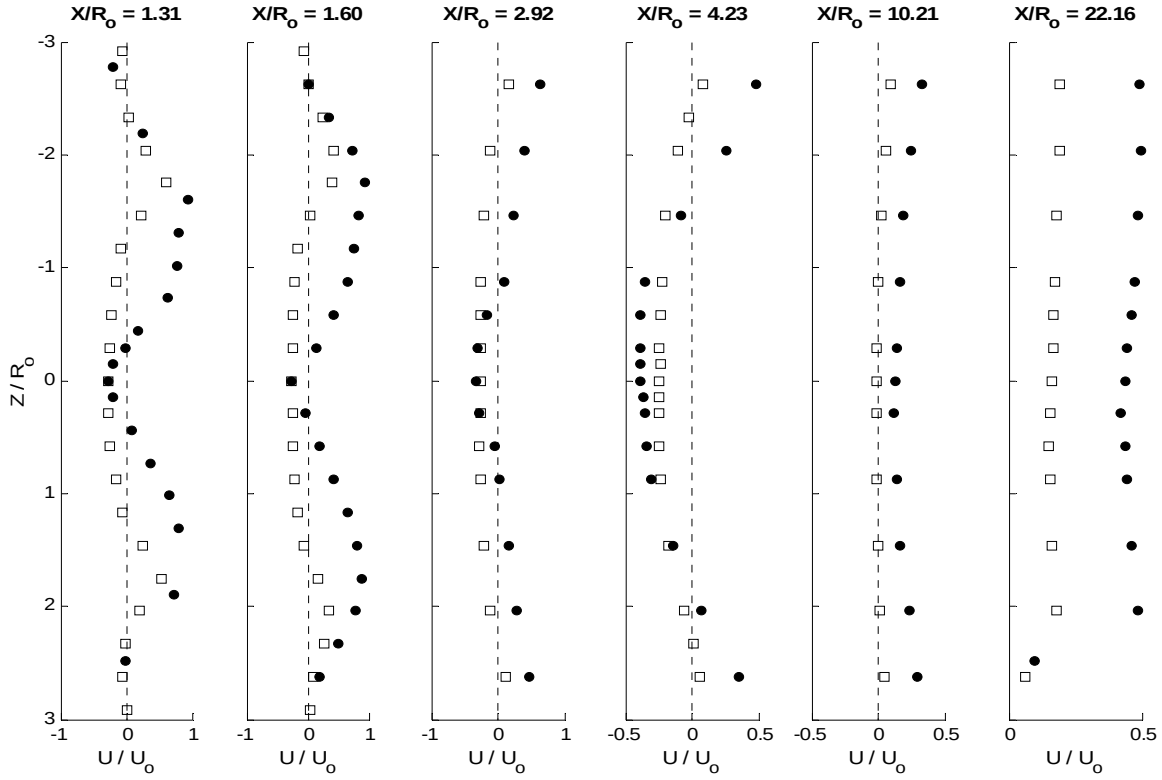

Figure 3. Axial mean velocity horizontal centerline downstream. (Legend, see Fig. 2)

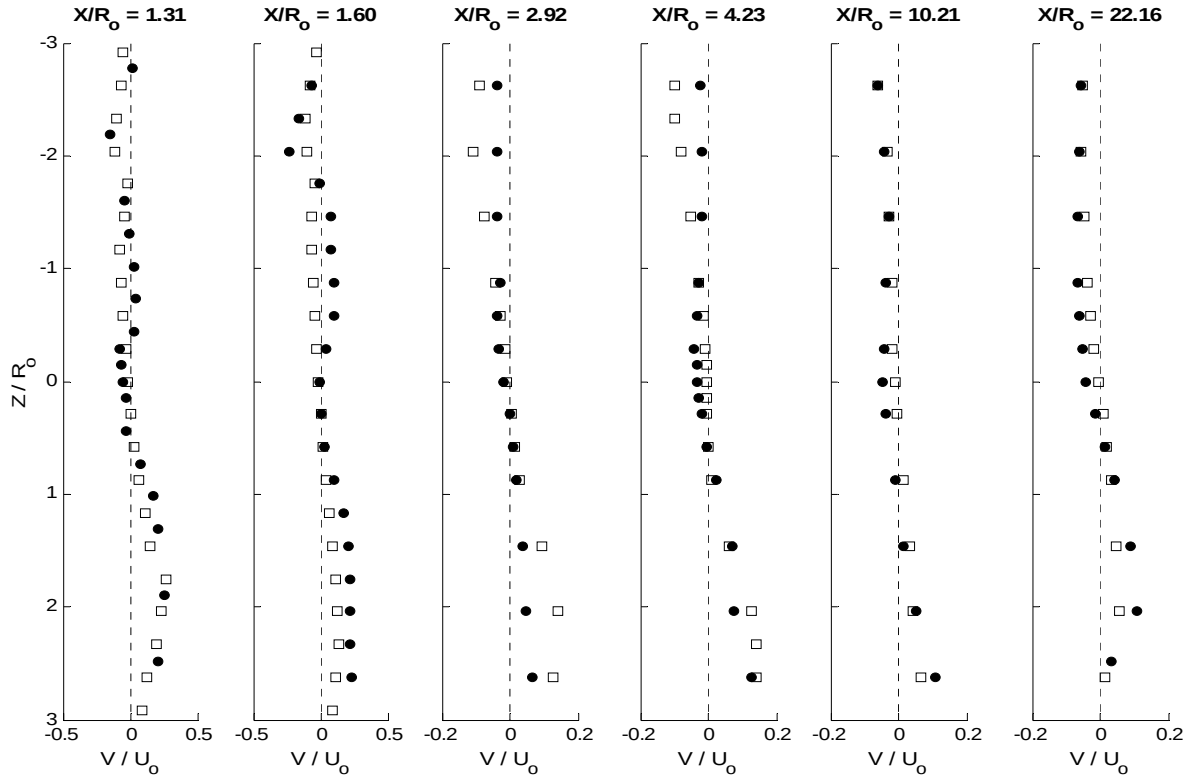

Figure 4. Vertical mean velocity horizontal centerline downstream. (Legend, see Fig. 2)

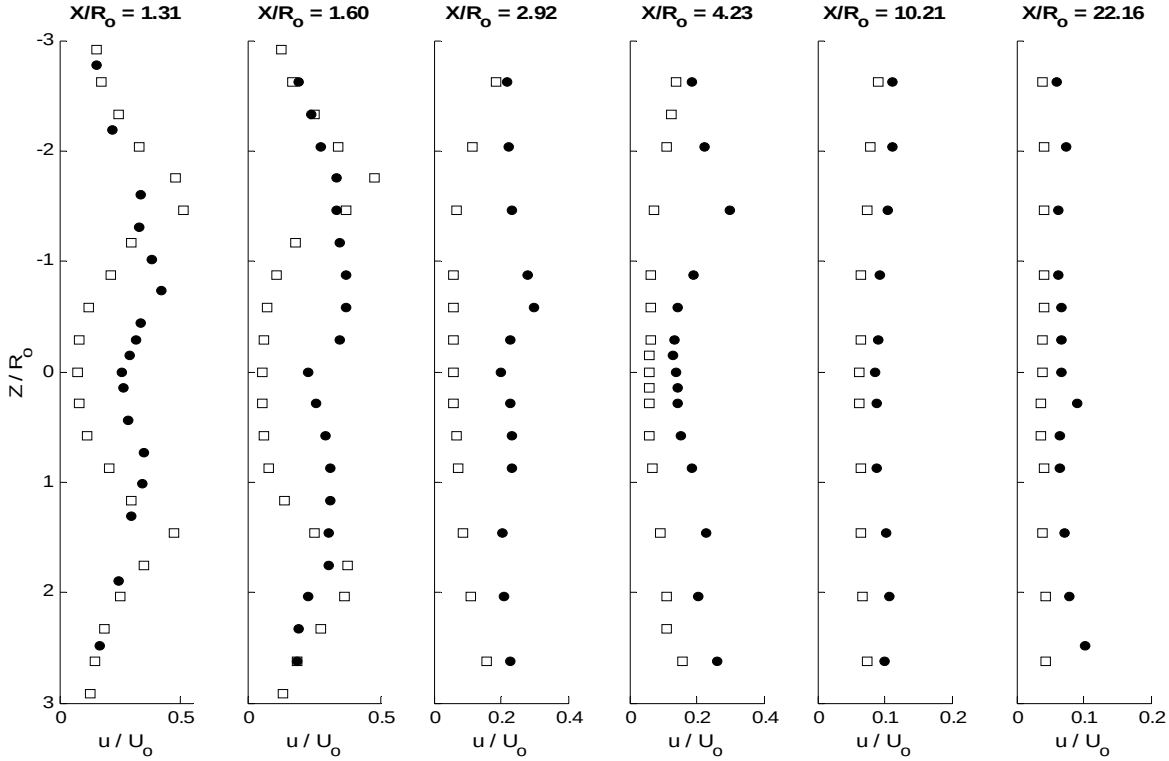

Figure 5. Axial rms velocity horizontal centerline downstream. (Legend, see Fig. 2)

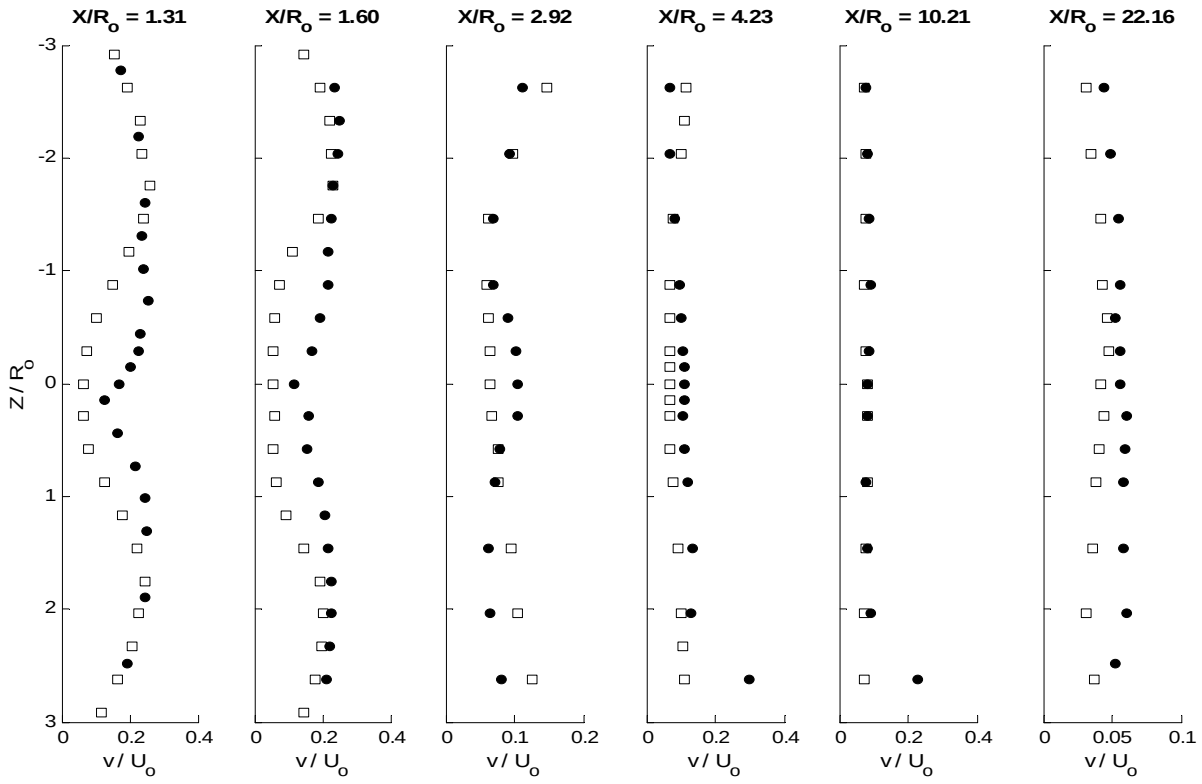

Figure 6. Vertical rms velocity horizontal centerline downstream. (Legend, see Fig. 2)

C. Near Injector Turbulence

Two-dimensional turbulence measurements in the near injector-region are presented in Fig. 7 and Fig. 8. Both the time averaged turbulent kinetic energy (TKE), as defined in Eq. (2), and the Reynolds shear stress were measured for the non-reacting and reacting gas phase using the TSI LDV coincidence mode. In this mode, valid signals occur only when fringes on both channels register the same particle crossing, providing the necessary correlation for higher order velocity statistics.

$$k = \overline{u'^2} + \overline{v'^2} \tag{2}$$

The 2-D TKE measurements, shown in Fig. 7, agree well with similar results for swirling flows[10,11,13]. At X/R_o = 1.31, the non-reacting TKE is contained in small regions on both sides of the swirl burner. This confinement is expected, as the maxima of the rms velocity components are located in a similar region. By X/R_o = 1.60, the peaks in the TKE are shifted outwards, as the vortex breakdown bubble widens. This broadening continues to X/Ro = 2.92 where the maxima are seen in the flow periphery. These peaks clearly show an increase in turbulent mixing associated with the shear layer at the recirculation boundaries, a key feature of aerodynamic swirl stabilization.

Heat release changes the gas phase TKE significantly. At X/R_o = 1.31, similar maxima are clear, but with reduced magnitude. These maxima, however, can be attributed to the liquid-spray interactions near the nozzle, dominated by the spray angle and SMD of the droplets. As droplets enter the combustion chamber with a large amount of counter-rotation relative to the mean flow, they are generally unable to follow the existing flow. Instead, these droplets follow a trajectory through the mean flow, generating significant amounts of turbulence near the injector. Research has also shown that, in the near-injector region of spray flames, external, or sheath type, combustion modes are common[14]. This sheath type combustion mode is characterized by many unburned droplets surrounded by a gaseous diffusion flame, which agrees well with the results shown. Unburned droplets in the core of the spray contribute significantly to the 2-D TKE, while combustion at the spray periphery reduces the turbulent intensity. Downstream, at X/R_o = 1.60, as the evaporation and the mixing processes become important, the TKE distribution is seen to broaden. As the initial droplet momentum is decreased due to drag forces on the droplets,

mixing and diffusion characteristics are improved. With this improved mixing, and the convection of droplets outward due to volumetric expansion, the TKE is spread across the combustor, with values increasing at the spray periphery and centerline, while decreasing in the core regions. This implies that the droplet penetration is reduced downstream, while radial diffusion is increased. Further downstream, at X/R_o = 2.92, the TKE is dramatically reduced. This reduction is due to the partial relaminarization of the flow at high combustion temperatures[15]. At this distance downstream, evaporation and mixing have had a significant impact, and combustion occurs in both the gas/droplet and droplet phase[14]. Combustion is more complete across the chamber cross section and a more uniform temperatures distribution is expected. Consequently, turbulence fluctuations are reduced, as is the turbulent energy at small scales[15].

Figure 8 shows the normalized, 2-D, time averaged Reynolds shear stress and vertical gradient of the axial mean velocity at X/R_o = 1.60 for both the non-reacting and reacting gas phase. The normalization parameters are:

$$u^* = k^{1/2}, \quad l_m = 0.65\, R_o \tag{3}$$

Measurements along the vertical centerline enable the calculation of the vertical gradient of the axial mean velocity, necessary to examine the validity of a turbulent viscosity model. For a simple shear flow, this viscosity is given[16]:

$$\upsilon_T = -\overline{u'v'} \,/\, (dU/dy) \tag{4}$$

When the turbulent viscosity is positive, gradient diffusion dominates and the flux of turbulent kinetic energy is towards the smaller scales. However, when this turbulent viscosity is negative, the flow of energy is towards the large scales. The correct choice of a model is pivotal for the success of numerical simulations, and the validity of a gradient diffusion model for counter-swirl combustion modeling is addressed below.

From the non-reacting results, it is clear that in the main shear layer, the gradient diffusion model is correct, and the turbulent viscosity is positive. In the core region, the normalized shear stress appears much larger than the mean gradient. This suggests the transport of turbulent momentum from the core to the shear layer, followed by

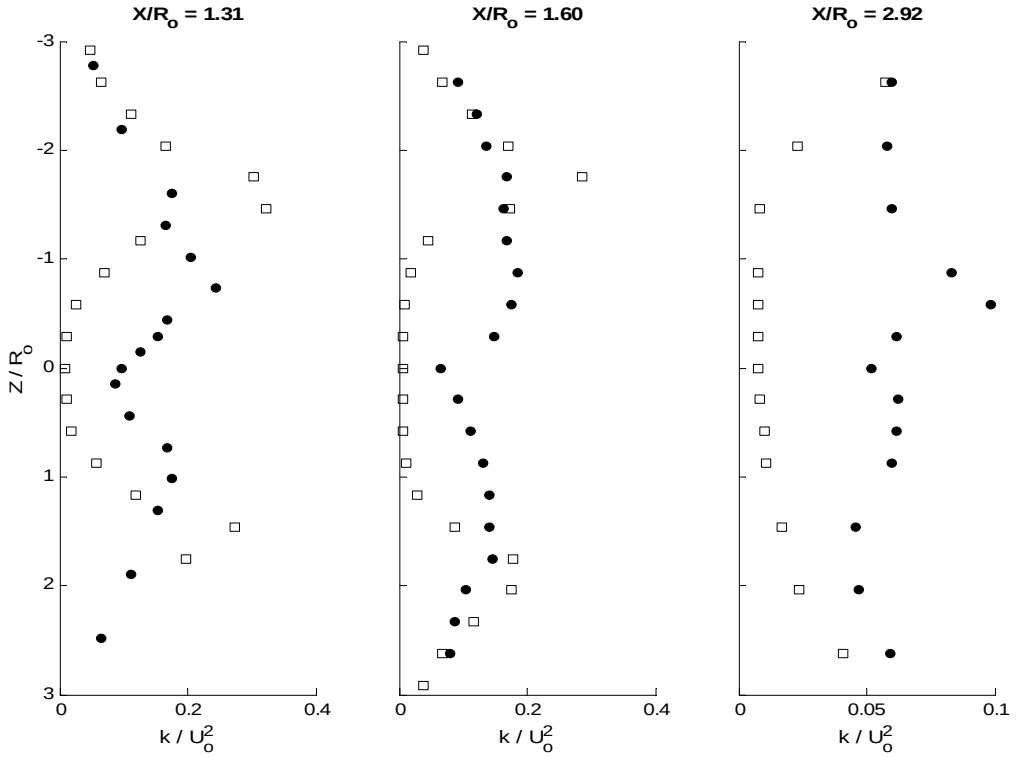

Figure 7. Turbulent kinetic energy horizontal centerline in the near nozzle region. (Legend, see Fig. 2)

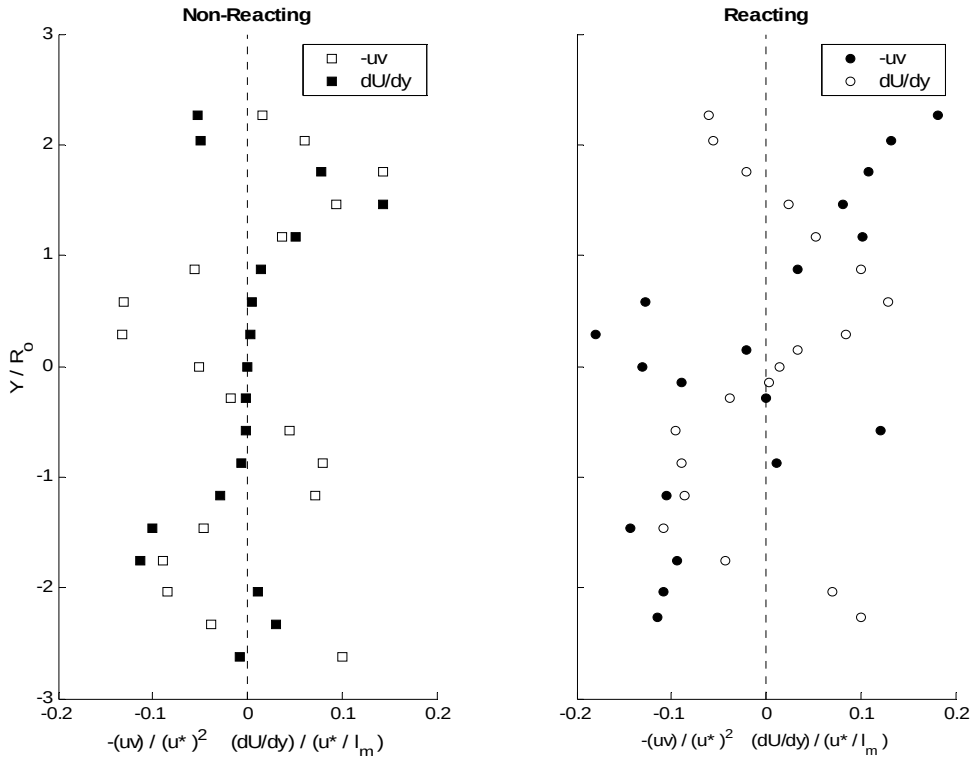

Figure 8. Reynolds shear stress and axial mean velocity gradient vertical centerline, $X/R_o = 1.60$.

the active diffusion of this momentum across the shear layer. These results agree well with work that showed an increase in the radial flux of axial momentum for non-reacting counter-swirl flows[9].

With the addition of heat, the second order correlation measurement does not agree with the vertical mean velocity gradient, and shows significant asymmetry. The substantial differences in behavior suggest that a gradient diffusion model may not capture the turbulent momentum transport of this flame. Instead, the increase in the vertical gradient strength near $Y/R_o = 0$ and the addition of the liquid phase inhibit the diffusion of energy to the small scales. This result is consistent with Fig. 7; a rise in the transport of turbulent momentum coupled with a decrease in the dissipation. The asymmetries in this second order correlation are due in part to the increased uncertainty associated with measuring higher order statistics in the turbulent flame, and also in part to the asymmetric nature of the combustion.

D. Non-Reacting/Reacting Droplet Comparison, $X/R_o = 1.60$

The droplet SMD, defined in Eq. (1), normalized to the rated fuel nozzle SMD, is shown in Figure 9 for both the reacting and non-reacting droplets across the combustor horizontal centerline. Notice that for the non-reacting case, the droplet SMD remains nearly constant, roughly 75% of the nozzle's rated SMD. This behavior agrees well with results shown[17], where constant SMD values across a symmetric spray tube diameter were observed. For the reacting case, the large SMD in the spray periphery, as well at $Z/R_o \sim -0.75$, is of prime importance. In these regions, the droplet SMD is over three times the rated SMD. This behavior is significant, as it does not agree with previous research[12,17]. In earlier studies, co-annular swirl was considered in axi-symmetric combustors. In addition to these differences, the fuel type and equivalence ratios were different from those used here.

These large SMD values can be explained if the fuel nozzle's spray characteristics are examined in detail. At operational fuel pressure, the nozzle should produce a hollow conical spray with rated spray angle and droplet size, given above. However, at lower fuel pressures, these conditions will not be satisfied. Instead, the spray angle will decrease, and the average droplet diameters will increase[1]. When the design geometry is considered, along with the low operating fuel pressure, the decrease in spray angle may explain the results presented below. Without combustion, the larger droplets still impinge on the venturi lip, and are re-atomized at the swirl interface. This process creates nearly uniform droplets independent of spray behavior. However, with the flow expansion

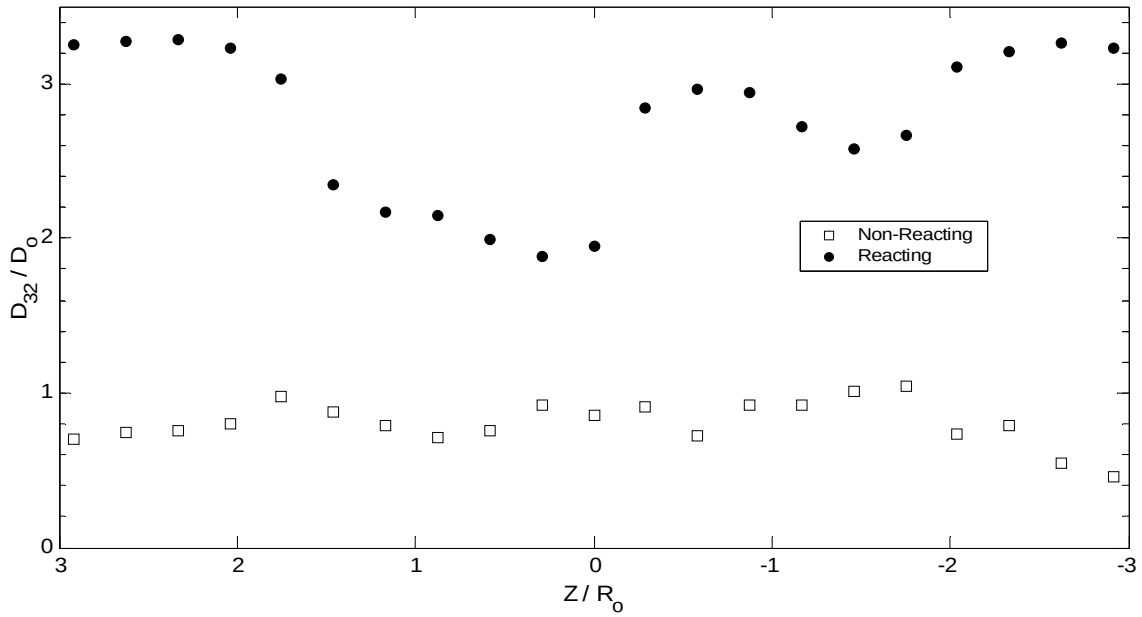

Figure 9. Normalized droplet SMD comparison horizontal centerline, $X/R_o = 1.60$.

associated with the release of heat, the large droplets no longer impinge on the venturi lip, instead convecting downstream into the main recirculation region. It does appear that some of the droplets are re-atomized at the primary/secondary swirl boundary, seen in the SMD reduction near $Z/R_o = 1$.

To further justify the large droplet diameters presented, the effects of group combustion in sprays must be examined. As described by Chiu, the "group combustion phenomenon is induced by the droplet state modulation as the result of collective interaction in a many-droplet system.[14]" Of particular importance is the formation of large scale structures (LSS), "non-homogeneous structures such as clusters, clumps, or non-coherent structures of high droplet population.[14]" Immediately downstream of the fuel nozzle, the inherent ligaments and clusters due to initial breakup tend to coalesce, which further accelerates the production of these LSS. It was further observed that if the dispersed phase momentum is greater than the global gas phase momentum, the "rate of relaxation will be slow and the LSS will have a prolonged life time.[14]" Thus, the results presented in Fig. 9 agree well with theoretical predictions for practical spray combustion. The evidence of large structures is clear in the increased SMD. In these regions of large SMD it is reasonable to assume that both the sheath type (group) combustion mode and droplet coalescence play pivotal roles in the formation of large droplets. Since the disperse phase momentum is larger than the global gas phase momentum in these experiments, the slow downstream decay of these structures is expected. While these results do not agree with previous co-swirl experiments, they are explained under a group, or hierarchal, combustion mode with significant large scale structure formation.

To further quantify the differences between the non-reacting and reacting droplets, Fig. 10 and Fig. 11 show the mean axial and vertical velocities for both the non-reacting and reacting liquid phase. It is clear that heat release, and the associated volumetric expansion, have a major effect on droplet velocities. In the reacting case, mean axial droplet velocities exceed the non-reacting droplet velocities across the entire combustor, except near the combustor walls (see Fig. 10). This behavior is as expected, as droplets are accelerated throughout the flow due to the energy liberated during combustion. The asymmetric fuel spray is further seen in the increased axial mean velocities for $Z/R_o < 0$. The larger reacting droplets (see Fig. 9), follow the spray trajectory, traveling more rapidly through the gas phase.

In Fig. 11, the flow acceleration associated with combustion has a significant impact on the droplet vertical mean velocity. For the non-reacting liquid phase, the impact of the counter-swirl is negligible by $X/R_o = 1.60$. However, the reacting droplets show substantial counter-swirl at the same location. This seeming inconsistency is explained with consideration of the flow acceleration aforementioned. With the addition of heat, and the subsequent flow expansion, the region of intense counter-swirl is displaced downstream. This displacement is responsible for the trends shown in Fig. 11. For the non-reacting case, the counter-swirl behavior expected is upstream of $X/R_o = 1.60$. With combustion, however, the region of counter-swirl is clearly visible at $X/R_o = 1.60$. Thus, the downstream convection of the main counter-swirl region is attributed to the volumetric expansion of the flow. It is also clear that this counter-swirl is not symmetric, in agreement with the previous results concerning the asymmetric spray field.

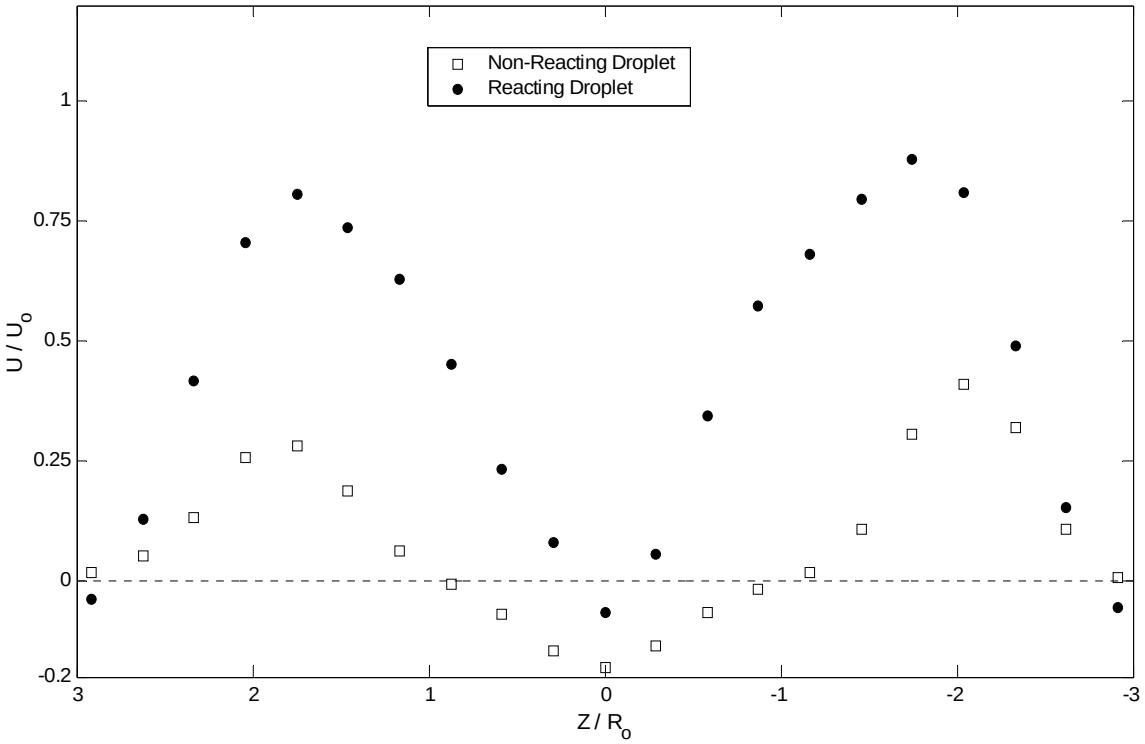

Figure 10. Axial mean velocity comparison horizontal centerline, $X/R_o = 1.60$.

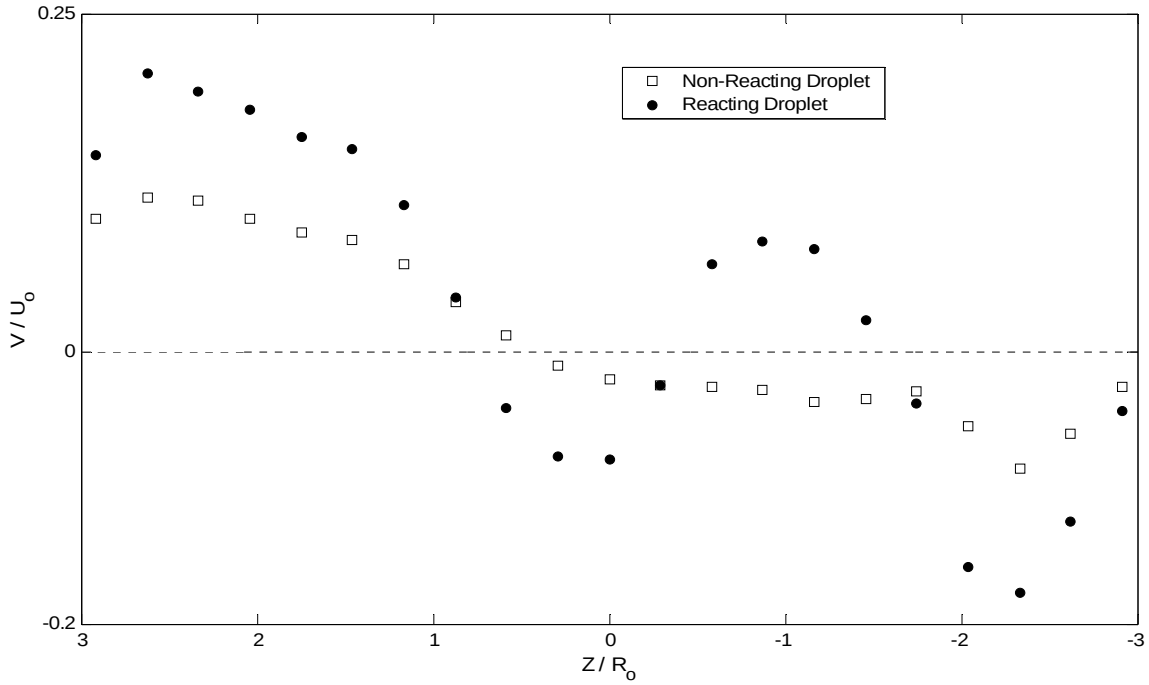

Figure 11. Vertical mean velocity comparison horizontal centerline, $X/R_o = 1.60$.

E. Exhaust Gas Measurements

Both combustion exhaust composition and temperature were measured downstream of the exhaust section, $X/R_o = 22.20$. Specific attention is given to the NO_x and CO concentrations, each corrected to 15% O_2, shown with the combustion product temperature in Fig. 12. The asymmetric combustion described above is clear, as exhaust temperature changes dramatically across the exhaust section. For $Z/R_o > 0$, the combustion temperatures were low, evidence of complete combustion upstream. Further, the low NO_x and high CO concentrations agree well with low product temperature. From Fig. 9 above, this region also had the smallest reacting droplet SMD values. Thus, the smaller droplets were able to evaporate, mix, and burn more efficiently, reducing the flame length. As a result, the exhaust temperatures and NO_x concentrations are reduced.

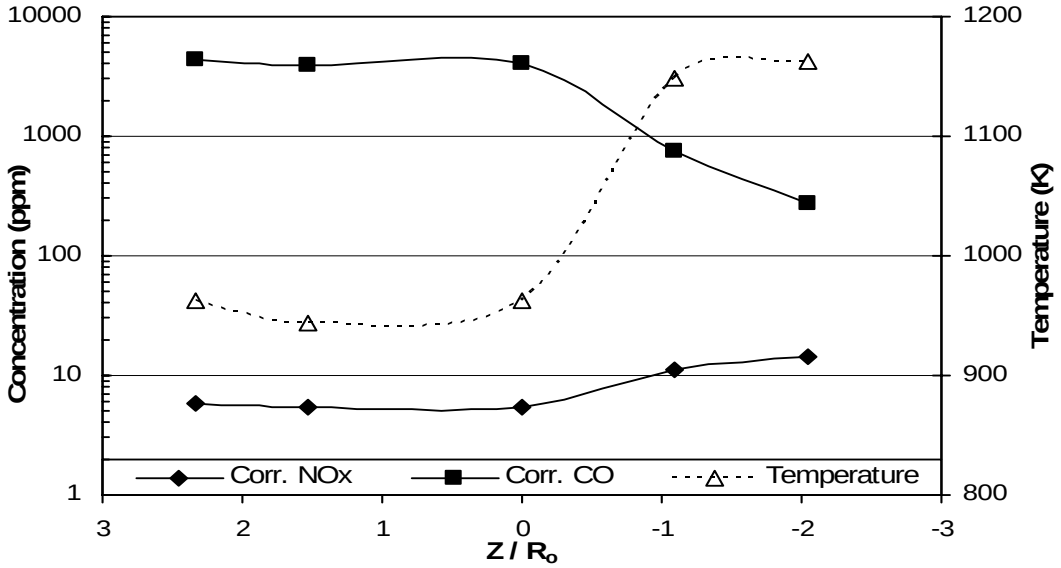

Figure 12. Exhaust gas composition and temperature horizontal centerline.

While the previous results agree well with lean, low NO_x combustion, results for $Z/R_o < 0$ are not ideal. The corrected NO_x concentrations are above 10ppm, while the exhaust temperatures approach 1200 K. In this region, as shown in Fig. 9-11, larger reacting droplets with increased velocities are unable to burn completely, and as such, combustion continues farther downstream. This increase in the flame length directly leads to the increase in temperature shown in Fig. 12. With this increase in product temperature, the CO concentration decreases while the NO_x increases, in good agreement with previous work[1].

IV. Conclusion

The existence of a large vortex breakdown bubble, typical of high swirl flows, is clear in the non-reacting gas phase flow. This breakdown bubble is characterized by a large area of recirculating flow, responsible for the convection of gas downstream to the near-injector region. Along with enhanced mixing in the resulting shear layer, this mechanism plays a key role in both flame stabilization and combustion efficiency. The volumetric expansion associated with the addition of heat due to combustion constricts this vortex bubble, reducing the length and width while increasing the core velocity magnitude. Similarly, the mean axial velocity is increased significantly, as are the turbulent properties. Droplet diameter measurements suggest that the non-reacting droplets lose the primary counter-swirl rapidly, instead follow the secondary swirl imparted at the venturi lip downstream. With combustion, however, the reacting droplets do show the primary counter-rotation as the volumetric expansion convects these structures downstream. Finally, asymmetric burning due to the poor fuel spray characteristics is evident. Future studies will specifically address this asymmetry by using another fuel spray injector that is designed for atmospheric pressure operation.

Acknowledgments

The author gratefully acknowledges the support of GE Transportation, under the University Strategic Alliance (U.S.A.) project, contract number 200-10-14R53108. Hardware and technical support is also appreciated. The support of NASA/ARC is acknowledged as well; contract number NAG 2-1615.

References

[1]Lefebvre, A. H., *Gas Turbine Combustion*, 2nd ed., Taylor & Francis, Philadelphia, PA, 1999.

[2]Nair, S., et al., "Lean Blowout Detection in a Single Nozzle Swirl Cup Combustor," *42nd AIAA Aerospace Sciences Meeting and Exhibit*, AIAA, Washington, DC, 2004, pp. 3437-3448.

[3]Menon, S., Patel, N., "Subgrid Modeling for LES of Spray Combustion in Large-Scale Combustors," *AIAA Journal* (to be published).

[4]Chevron Phillips, Chemical Company LP, Certificate of Analysis, mfg date: 07/2004.

[5]Phase Doppler Particle Analyzer (PDPA)/Laser Doppler Velocimeter (LDV) Operations Manual, TSI Inc., St. Paul, MN, 2001.

[6]Instruction Manual for PG-250 Portable Gas Analyzer, Horiba Instruments Inc., Irvine, CA, 1997.

[7]Chigier, N. A., and Beér, J. M., *Combustion Aerodynamics*, John Wiley and Sons, Inc., New York, 1972.

[8]Syred, N., and Beér, J. M., "Effect of Combustion Upon Precessing Vortex Cores Generated by Swirl Combustors," *Fourteenth Symposium (International) on Combustion*, The Combustion Institute, Pittsburgh, PA, 1973 pp. 537-550.

[9]Merkle, K., Haessler, H., Büchner, H., and Zarzalis, N., "Effect of co- and counter-swirl on the isothermal flow- and mixture-field of an airblast atomizer nozzle," *International Journal of Heat and Fluid Flow*, Vol. 24, 2003, pp. 529-537.

[10]Hsiao, G., Mongia, H., and Vij, A., "Swirl Cup Modeling Part II: Inlet Boundary Conditions," *41st AIAA Aerospace Sciences Meeting & Exhibit*, AIAA, Washington, DC, 2003.

[11]Hsiao, G., Mongia, H., and Vij, A., "Swirl Cup Modeling Part III: Grid Independent Solution with Different Turbulence Models," *41st AIAA Aerospace Sciences Meeting & Exhibit*, AIAA, Washington, DC, 2003.

[12]Bulzan, D. L., "Velocity and Drop Size Measurements in a Swirl-Stabilized, Combusting Spray," *SPIE-The International Society for Optical Engineering*, Vol. 1862, 1993, pp. 113-122.

[13]Owen, F. K., "Measurements and Observations of Turbulent Recirculating Jet Flows," *AIAA Journal*, Vol. 14, No. 11, 1976, pp. 1556-1562.

[14]Chiu, H. H., "Progress and Challenges in Droplets and Spray Combustion," *ASME Asia '97 Congress & Exhibitions*, ASME, New York, 1997.

[15]Karpetis, A. N., and Gomez, A., "An Experimental Study of Well-Defined Turbulent Nonpremixed Spray Flames," *Combustion and Flame*, Vol. 121, 2000, pp. 1-23.

[16]Pope, S. B., *Turbulent Flows*, Cambridge University Press, Cambridge, England, UK, 2001.

[17]Bossard, J. A., and Peck, R. E., "Droplet Size Distribution Effects in Spray Combustion," *Twenty-Sixth Symposium (International) on Combustion*, The Combustion Institute, Pittsburgh, PA, 1996 pp. 1671-1677.